Three-dimensional arrays of submicron particles generated by a four-beam optical lattice

B. N. Slama-Eliau and G. Raithel

Phys. Rev. E **83**, 051406 — Published 31 May 2011

DOI: 10.1103/PhysRevE.83.051406

Three-dimensional arrays of sub-micron particles generated by a four-beam optical lattice

B. N. Slama-Eliau and G. Raithel*

FOCUS Center, Department of Physics,

University of Michigan, Ann Arbor, MI 48109

Abstract

Using an optical lattice formed by four laser beams, we obtain three-dimensional light-induced crystals of 490 nm diameter polystyrene spheres in solution. The setup yields face-centered orthorhombic optical crystals of a packing density of about 40%. An alignment procedure is developed in which the crystals are first prepared near a sample wall, and then in the bulk of the sample. A series of tests is performed that demonstrate particle trapping in all three dimensions. For one case, the trapping force is measured, and good agreement with a simple theoretical model is found. Possible applications are discussed.

PACS numbers: 42.50.Wk, 87.80.Cc

* graithel@umich.edu

I. INTRODUCTION

We have realized artificial crystals of sub-micron particles in solution. In contrast to crystals in the usual sense, these are non-frozen, periodic particle assemblies held together by the optical forces generated by an optical lattice. Optical lattices are formed by the interference of multiple intersecting, coherent laser beams. Sub-wavelength-sized particles immersed in the field get trapped at periodic lattice sites due to the electric polarizability of matter. This trapping method is widely applied to atoms in a vacuum environment [1, 2] as well as to mesoscopic particles in solution. The light force consists of a "scattering force", which is proportional to the intensity and pushes the particle in the direction of the incident light, and a "gradient force", which is proportional to and in the direction of the intensity gradient [3, 4]. Stable traps, or optical tweezers, are realized when the gradient force is larger than the scattering one [5]. Single-particle optical tweezers have proven useful in a remarkable number and range of applications [6, 7]. Their versatility has further increased with the realization of multiple trapping sites. Schemes have been developed that provide a large number of periodic one-dimensional (1D) traps [8] or complex 2D and 3D arrangements of traps. To accomplish that, split laser beams can be recombined in multi-purpose interference patterns [9–13] or first be resculpted using holographic techniques [14–18].

While the scattering force is essential in implementing laser cooling of atoms [19], it generally hampers the trapping of mesoscopic particles in solution at room temperature ($T = 300$ K). There, the gradient force must be large enough to outweigh the scattering force, and the potential that underlies the gradient force must be deeper than $k_{\mathrm{B}}T$ to localize the particles against the Brownian motion. For single-site optical tweezers, a microscope objective with high numerical aperture (NA) is required to bring the laser beam to a tight focus, thereby creating a large axial gradient force capable of counter-balancing the axial scattering force. In multiple-site tweezers, several smaller-diameter laser beams may be introduced into a microscope objective to form an optical lattice at the focal plane. The effective NA of those beams is then necessarily diminished, and the gradient force at the focal point is no longer sufficient to counter-balance the forward scattering force. This problem has been addressed, for example, by adding a counter-propagating beam [6], or by using highly reflective optics [8, 20]. In some experiments, the scattering force was left

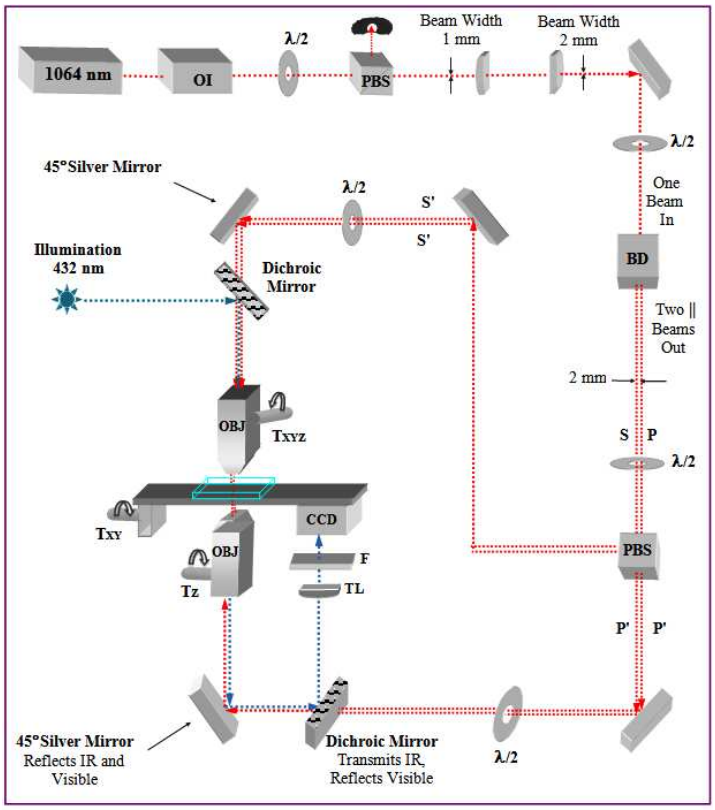

FIG. 1. (Color online) Sketch of the experimental setup. OI = optical isolator, $\frac{\lambda}{2}$ = half-wave plate, PBS = polarizing beam splitter, BD = beam displacer, OBJ = objective, Tz, Txy, Txyz = translation stages, TL = tube lens, F = filter.

unbalanced, in which case the particles were pushed against a sample wall, leading to traps of reduced dimensionality.

In this work we generate optical crystals of sub-micron particles using an optical lattice formed by four laser beams. The beam geometry is highly symmetric and therefore conducive to the achievement of radiation pressure equilibrium, which is essential in obtaining stable, 3D optical crystals away from the cell walls. An important property of the four-beam geometry is that phase variations of the trapping beams only result in lattice translations, but not in a change of lattice structure or a loss of trapping functionality. This property leads to an intrinsic stability of the lattice against random phase drifts of the lattice beams. It further provides us with the opportunity to manipulate the particle positions via phase control. The setup is economical and efficient, as four is the smallest possible number of lattice beams that can generate 3D periodic arrays of optical traps. The obtained optical crystals have an approximately face-centered orthorhombic structure, are quite densely packed, and can be

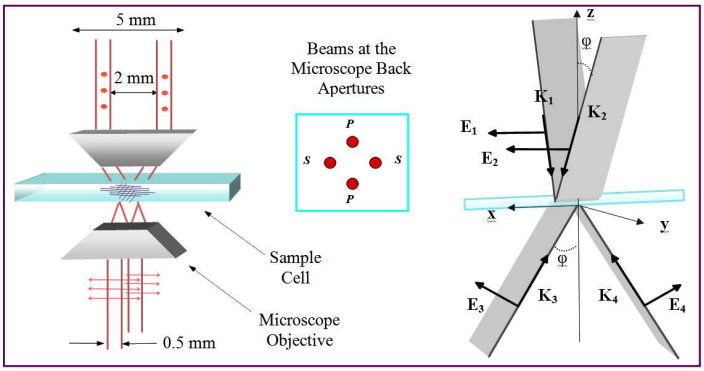

FIG. 2. (Color online) Schematic of the four-beam lattice geometry for s-polarized down-going and p-polarized up-going beams. Left: Overview showing the microscope objectives, lattice beams and sample cell. Middle: Cross-sectional view of the lattice beams at the microscope back apertures. Right: propagation and field vectors at the confocal point.

formed remotely from the cell walls.

II. EXPERIMENTAL SETUP

A sketch of the experimental setup is shown in Fig. 1. A birefringent calcite crystal splits the beam of a continuous-wave Nd:Yag fiber laser (wavelength $\lambda_0 = 1064$ nm) into two parallel beams of orthogonal polarizations, with a fixed separation of 2 mm. Those beams are further split into four by a polarizing beam splitter, which steers two beams upward, while the other two remain in a lower horizontal plane. The upper and lower beam pairs are directed down or up via silver mirrors into the backs of two identical 100X, infinity corrected microscope objectives of 1.25 NA and 60% transmission at 1064 nm. The objectives are confocally aligned and have a common optical axis. All four laser beams have approximately the same power and travel nearly the same length from the beam splitters to the sample. The beam polarizations and intensities are controlled using several half-waveplates, shown in Figure 1. A high degree of symmetry is provided by making sure that all beams propagate parallel to and at equal distances (of 1 mm) from the shared axis of the objectives. Furthermore, the distance between the objectives is adjusted so that the lattice beams enter and exit them at the corners of a square (see Figure 2). In this arrangement, a highly symmetric four-beam optical lattice is formed at the confocal point.

The sample cell is fabricated from two standard 170 μm microscope cover slips separated

by a 100 μm paraffin film. The cell contains an autoclaved water solution of 490 nm diameter polystyrene particles (Bangs Laboratories, refractive index $n_{\rm p} = 1.59$) at a concentration of about 10^7 particles/cm^3 with 0.05% v/w Tween 20 to prevent aggregation. Blue light from an LED (center wavelength 450 nm) illuminates the particles through the top objective, which acts as a condenser. The bottom objective and a tube lens of focal length 200 mm generate a 100X magnified image of the optical crystal on a CCD chip. Two dichroic mirrors that transmit the 1064 nm lattice laser beams and reflect visible light are used to separate the blue observation light from the infrared optical-lattice beams.

We have chosen to implement a four-beam setup similar to that shown in Figure 2, as detailed further in Sec. III, and with all beams p-polarized. The propagation vectors $\mathbf{K}_1$, $\mathbf{K}_2$ of the top and $\mathbf{K}_3$, $\mathbf{K}_4$ of the bottom pair of lattice beams form identical angles φ with the z-axis and satisfy $\sum_{\rm i=1}^{4} \mathbf{K}_{\rm i} = 0$. The wave-number $|\mathbf{K}_{\rm i}| = K = \frac{2\pi}{\lambda}$ with $\lambda = \lambda_0/n_{\rm w}$ and the refractive index of water $n_{\rm w} = 1.33$. The lattice periods are controlled via the angle φ, which in turn depends on the separation between the lattice-beam pairs at the 5 mm diameter back apertures of the microscope objectives. In the present experiment, the lattice beam separations are set to 2 mm by the birefringent crystal.

III. OPTICAL LATTICE DESIGN

A. Intensity distributions

In preparation for the experiment, we have calculated the intensities and the resultant trapping potentials for different directions and polarizations of the laser beams that form the optical lattice. We begin with calculating the intensity in the optical lattice, $I(\mathbf{r})$, as a function of position, $\mathbf{r}$, summed over all polarizations. For simplicity, we neglect the spatial variation of the single-beam intensities and the Guoy phase and choose beam directions as shown in Figure 2, with all beams having the same angle φ and intensity I_0. The up-going and down-going beam pairs are either s-polarized or p-polarized. For s-polarization (p-polarization), the beams have linear polarizations that are perpendicular to (in plane with) the plane formed by the respective beam pair. If all beams are s-polarized, the total intensity is

$$I_{\rm ss}(\mathbf{r}) = 2I_0[2 + \cos(2Kx\sin\varphi) + \cos(2Ky\sin\varphi)] \quad ,$$

which exhibits periodicity in x- and y-directions, but not in z. Hence, this case generates a 2D lattice but not a 3D one (assuming particles with isotropic polarizability). If one pair of beams is s-polarized and the other p-polarized, as in Figure 2, the intensity is:

$$\begin{aligned} I_{\mathrm{sp}}(\mathbf{r}) &= 4I_0[\cos^2(\varphi)\sin^2(Kx\sin\varphi) + \sin^2(\varphi)\cos^2(Kx\sin\varphi)] \\ &+ 4I_0\cos^2(Ky\sin\varphi) \\ &+ 8I_0\cos(\varphi)\cos(Ky\sin\varphi)\sin(Kx\sin\varphi)\sin(2Kz\cos\varphi) \end{aligned}$$

Finally, with all beams p-polarized, $I(\mathbf{r})$ becomes:

$$\begin{aligned} I_{\mathrm{pp}}(\mathbf{r}) &= 4I_0\sin^2(\varphi)[\sin^2(Kx\sin\varphi) + \sin^2(Ky\sin\varphi)] \\ &+ 4I_0\cos^2(\varphi)[\cos^2(Kx\sin\varphi) + \cos^2(Ky\sin\varphi)] \\ &- 8I_0\sin^2(\varphi)\sin(Kx\sin\varphi)\sin(Ky\sin\varphi)\cos(2Kz\cos\varphi) \end{aligned} \tag{1}$$

In the last two cases, the intensity patterns are periodic in x, y and z, corresponding to 3D optical lattices. The lattice periods are $a = b = \lambda/\sin\varphi$ in x- and y-directions, respectively, and $c = \lambda/(2\cos\varphi)$ in z-direction. The intensity for all beams p-polarized takes a particularly simple form when $\varphi = \pi/4$, which is the configuration targeted in our experiment:

$$I_{\mathrm{pp},\pi/4}(\mathbf{r}) = 4I_0[1 - \sin(Kx/\sqrt{2})\sin(Ky/\sqrt{2})\cos(\sqrt{2}Kz)]\,. \tag{2}$$

For all cases, one can easily show that phase shifts of the beams only result in overall translations of the intensity distributions. The lattice structure therefore is inherently stable against phase changes that occur over time scales that are longer than the response time of the trapped particles. Additionally, phase ramps applied to one or more lattice beams can be used to perform controlled translations of the trapped particles. Other methods of particle translations, not directly applicable to our setup, include ones that are based on holographic techniques (for a recent, sophisticated method see Ref. [21].)

B. Crystal structure

Since the particles are trapped at the maxima of the intensity, the crystal structure for the case described by Eq. 2, which is the one we targeted in the experiment, is revealed by identifying all locations where the product $\sin(Kx/\sqrt{2})\sin(Ky/\sqrt{2})\cos(\sqrt{2}Kz)$

$= -1$. Straightforward analysis shows that the lattice structure is face-centered orthorhombic (FCO), with the sides of the orthorhombic elementary cell parallel to the coordinate directions x, y, and z shown in Fig. 2. The respective side lengths of the elementary cell, denoted a, b and c, are $a = b = \sqrt{2}\,\lambda$ and $c = \lambda/\sqrt{2}$, and its volume is $\sqrt{2}\lambda^3$.

In the experiment, the optical crystals are observed via one of the microscope objectives from the z-direction. Hence, the observed, apparent lattice structure corresponds to that of the FCO lattice projected onto the xy-plane. In the observed two-dimensional projections of the optical crystals we expect to find square crystals with apparent side lengths $p_{\mathrm{x}} = p_{\mathrm{y}} = a/2 = \lambda/\sqrt{2} \approx 570$ nm. Particles that appear as nearest neighbors in the xy-projection of the crystal are offset from each other along the line of sight (*i.e.* the z-direction) by a distance $\frac{\lambda}{2\sqrt{2}} \approx 280$ nm. This z-displacement is so small that it is not (easily) detectable in microscopic images of the crystal. The true three-dimensional distance between particles that appear as nearest neighbors in the xy-projection is about $\sqrt{(\frac{\lambda}{\sqrt{2}})^2 + (\frac{\lambda}{2\sqrt{2}})^2} \approx 630$ nm. Particles with identical x- and y-positions that are stacked up along the z-direction have a separation of $c = \lambda/\sqrt{2} \approx 570$ nm. If several particles are stacked up in z-direction, some of them will be hidden and/or slightly out of focus in microscopic images of the crystal. This results in the impression of one "larger than usual" particle, as seen in several of the figures below.

C. Lattice volume

In this work we have used laser powers, summed over all four beams, of up to about 400 mW, limited by the damage threshold of the microscope objectives. At a fixed power, there is a tradeoff between lattice volume and light intensity within that volume. A suitable compromise is found by varying the lattice beam diameters at the back apertures of the microscope lenses. Smaller beam diameters correspond to smaller effective NA for the beams, larger focal spot sizes and hence a larger lattice volume, and lower intensities and hence a lower trapping force. We seek a beam diameter that leads to a satisfactory lattice volume while still providing efficient particle trapping.

The numbers of lattice planes, N_{x} and N_{y} in the x- and y-directions, are given by the apparent lattice periods and the spot size w of the lattice beams at the confocal point: $N_{\mathrm{i}} \approx w/p_{\mathrm{i}} = 2w \sin\varphi/\lambda$ ($i = x$ or y). We have targeted values of $N_{\mathrm{x}} \approx N_{\mathrm{y}}$ in the range

of five to ten. With $\sin\varphi$ of order 0.5, we seek a spot size w of order 5 μm, or about ten times the microscope resolution at 1064 nm. The desired diameter of each beam at the back aperture of the objectives is therefore about 0.5 mm, *i.e.* one-tenth of the back aperture diameter. To achieve that, a short 1:2 telescope is mounted approximately at the midpoint between the laser aperture and the microscope objectives. The telescope images the 1 mm diameter laser beam into 0.5 mm diameter collimated beams at the back apertures of the objectives. With these parameters, a lattice featuring of order one hundred stable sites is realized. We find that the trapping force for this lattice size is still sufficiently large to provide stable trapping.

IV. EXPERIMENTAL RESULTS

To realize 3D optical crystals experimentally, we devised a three-step protocol. First we form a 1D lattice using a single pair of beams focused downward onto the bottom wall of the sample cell. Next, we add the bottom-up pair of beams, also focused onto the bottom wall, resulting in a 2D crystal at the bottom wall. In the third step, the top and bottom objectives are raised by about 30 μm. This results in a 3D optical crystal in the interior volume of the cell, at a location where the scattering forces of all four beams approximately cancel. In the following, the steps are described in detail.

In the first step, we only use the top-down pair of beams (total power 80 mW to 150 mW). The beams are focused at the cell bottom, where they interfere and form a 1D lattice in y-direction (see Figure 3.A and B). The overall downward radiation pressure forces the particles to the cell bottom, thereby stabilizing the particles in z-direction. A fairly weak gradient force keeps the particles loosely bound in x-direction. The lattice loading typically proceeds as follows. When turning on the lattice beams, particles present in the beams and diffusing into them are pushed downward by the scattering force and are flushed into the interference region. There, they first form two distinct off-center 1D crystals at the perimeter of the interference region. This initial loading behavior is shown in Figure 3.A. Since the particles have to overcome increasingly higher potential barriers to fill the most stable sites near the center, it takes seconds to minutes for the crystals to equilibrate (Figure 3.B).

In the second step, a 2D lattice of beads in the xy-plane is formed by adding the bottom pair of beams, which propagate upward, as indicated in Figure 2. The focal positions of the

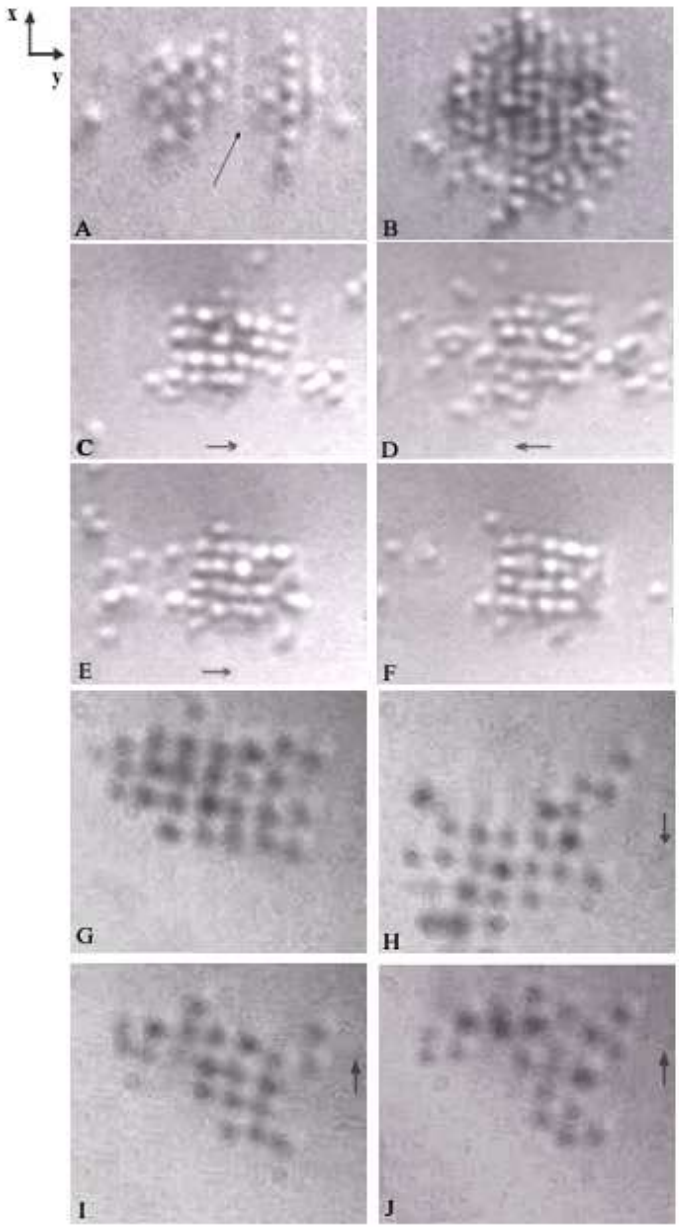

FIG. 3. Top: 1D crystals at the beginning of the filling process (A) and near steady-state (B). The arrow identifies the area where the lattice potential is deepest. The filling dynamics is explained in the text. C-F: Behavior of a 2D crystal during sample translation. Arrows indicate the sample motion relative to the lattice. Particles trapped in the central lattice region are retained, while unbound or loosely bound particles are flushed out during the sample translation. G-J: Behavior of a 2D lattice when scanning the relative phases of the lattice beams. The arrows indicate the direction of the phase-shift-induced motion of the lattice relative to the sample cell.

up- and down-going beams are adjusted such that there remains a weak downward radiation pressure that stabilizes the entire 2D crystal at the bottom sample wall. Interference now results in tight 2D trapping in both x and y at periodic lattice sites. The particles fill the lattice by hopping from site to site towards the center of the interference region, where the trapping potential is deepest.

To verify the effectiveness of 2D trapping, we performed several tests. First, we observe the formation and melting of the lattice by unblocking and blocking either pair of beams, or by gradually increasing or decreasing the total beam power. This verifies that all four beams are necessary to form the 2D lattice. The trapping in x- and y-directions is then probed via sample translations and lattice-beam phase shifts. In Figures 3.C to F, the sample is moved relative to the lattice at velocities of order 10 μm/s using a micrometer screw in y-direction, as indicated by arrows. The test is repeated for translation in x, using another micrometer screw. In either case, the beads near the crystal center remain trapped in the xy degrees of freedom against the drag forces induced by the sample motion. It is noted that particles that are not trapped or are only weakly trapped in the crystal perimeter are flushed out by the sample motion. Next, we introduce a thin microscope slide in the pathway of one of the lattice beams and slowly rotate it. The resultant phase shift causes a translation of the lattice planes relative to the stationary sample volume. The particles trapped in the lattice follow the motion of the lattice planes (Figures 3.G to J). This test also is conducted for both the x- and y-directions. All tests show that the trapping force in the 2D lattice exceeds the drag force for the velocities used.

In the third step, 3D optical crystals are formed in the bulk of the sample volume by raising the top and bottom objectives by 35 μm and 30 μm, respectively, resulting in corresponding upward translations of the focal spots of the beams into the interior of the sample cell. Typically, additional fine-tuning in the range of several microns is required in order to achieve a stable 3D bulk crystal. The 3D crystals were found to be relatively sensitive to beam imperfections. This is expected, as in the 3D case deviations from radiation pressure equilibrium are not "healed" by the presence of a sample wall (as is the case for the 1D and 2D crystals described above). We further find that the down-going beams need to focus several microns above the foci of the up-going beams for a stable trapping region to exist.

For the case of the 3D optical lattice, we have verified trapping in all three dimensions by performing tests similar to those used in the 2D lattice case. First, we block/unblock

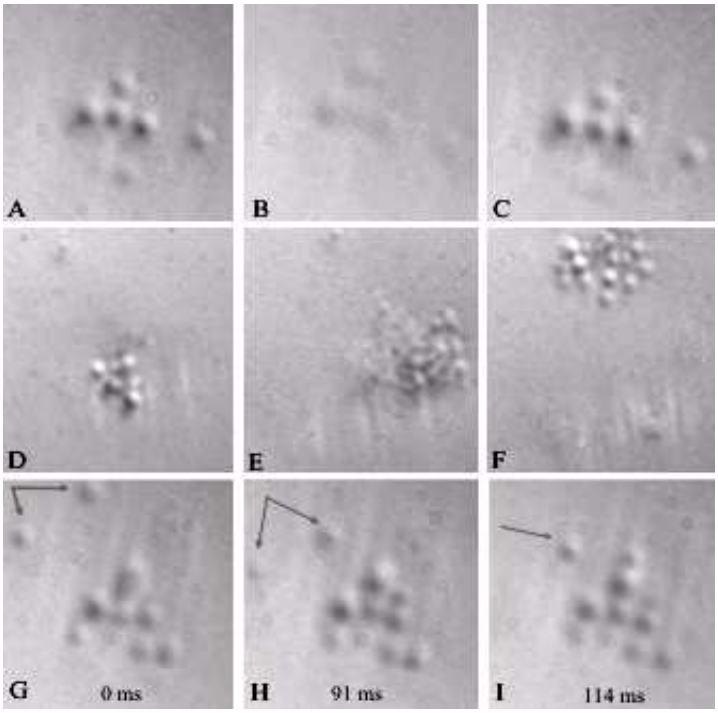

FIG. 4. Demonstration of 3D optical crystals in the sample bulk volume. A-C: Using lattice-beam phase shifts, the crystal is translated in observation (z) direction. As a result, the trapped particles come repeatedly in and out of focus, but their relative positions do not change. D-F: The particles are yanked out of the 3D lattice by jolting the sample. Comparing the numbers of particles visible in D and F, the z-stacking depth of the crystal in D is estimated to be at least three. In E, the particles appear out of focus because of their motion. G-I: Behavior of a 3D crystal during sample translation in the xy plane. The frame times are indicated. The trapped particles maintain their relative positions during the translation. The arrows identify two untrapped beads that move relative to those trapped. At 114 ms, one of them has become trapped in the lattice and one has moved away.

either the upward beams, or the downward beams, or both at the same time. In all cases, we observe melting/recrystallization of the crystal. Hence, all four beams are necessary to form the crystal. Next, we move the sample in the x- and y-directions using micrometer screws. The beads remain trapped in the lattice wells (Figures 4.G to I). To verify that the particles are locked in the z-direction as well, we introduce a 1 mm thick glass plate in the pathway of both down-going beams and slowly rotate it. As a result of the lattice-beam phase shifts, the beads move up and down in the z-direction while remaining locked relative

to one another. This is observed in Figures 4.A to C, where the same particle pattern repeatedly comes in and out of focus. Finally, to estimate how many particles are stacked along the z axis of the crystal, we gently jolt the sample. The resultant shake-up of the crystal exposes a considerable number of beads that were previously hidden in the depth of the crystal. Comparing Figures 4.D to F, we estimate that the stacking depth is at least three in that case.

To estimate the transverse gradient force, we have performed a standard Stokes' drag measurement [22, 23] at a total power of 350 mW, for the case of a 2D lattice formed at the bottom wall of the sample (as in Fig. 3.C-F). According to Stokes' law, a particle of radius R moving with speed v in a fluid of viscosity η experiences a friction force $F = 6\pi\eta Rv$. When the drag force on a trapped bead becomes larger than the opposing optical force, the bead escapes from the lattice. Ignoring negligible particle acceleration and thermal fluctuations, measurements of the particle escape speed yield the Stokes' force that equals the optical trapping force. In the experiment, we apply a linear voltage ramp to a piezoelectric actuator, which translates the sample cell in x-direction at a speed v_{x}. The number of particles trapped in the lattice is recorded at the beginning and at the end of the translation process. In Figure 5 we plot the measured escape fraction vs v_{x} and find an escape speed of $v_{\mathrm{x}} \approx 30$ μm/s. In the calculation of the optical trapping force from the escape speed, we account for the fact that the lattice is formed at the bottom wall of the cell by using an effective water viscosity triple to that in bulk solution (10^{-3} kg/(s m), see Ref. [23]). For our 245 nm radius beads, a trapping force of about 0.42 pN is found. This result is in line with values obtained for other beam geometries [5, 23] and agrees quite well with a theoretical estimate presented in the next section.

V. ANALYSIS

A. Packing density

A quantity of interest is the achieved packing density. A high packing density indicates that particle-particle interactions will be important, and that the optical crystal can possibly be tailored so that it exhibits a tunable photonic bandgap. In the present case, the optical crystals have FCO structure; hence, each elementary cell of a fully occupied crystal contains

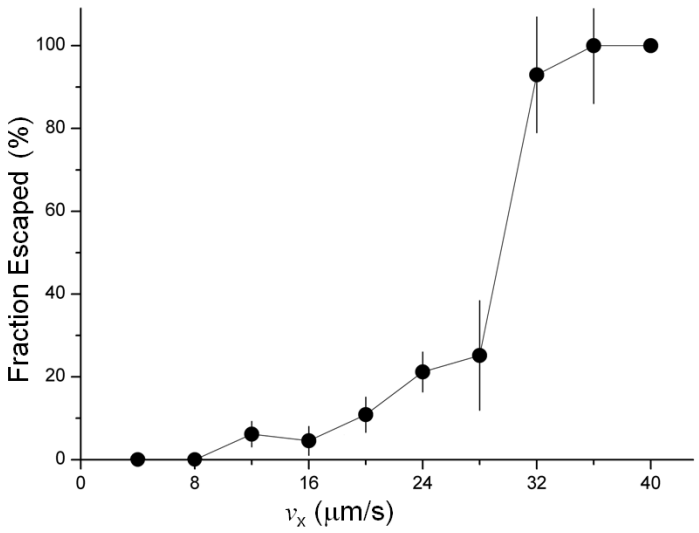

FIG. 5. Percentage of escaping particles vs translation speed. At a critical escape speed $v_x \approx 30$ μm/s, the escape percentage jumps from 25% to 90%.

four particles. For a lowest-order estimate of the filling fraction, we assume that the effective refractive index of the particle-filled medium is given by the volume average, *i.e.* $n_{\text{eff}} = [V_p n_p + (V - V_p) n_w]/V$, where V is the total elementary cell volume, and V_p is the particle-filled volume per elementary cell. This equation accounts for the fact that the effective refractive index is increased by the presence of the particles. For the packing density, V_p/V, we then solve the equation

$$\frac{V_p}{V} = \frac{V_p}{\sqrt{2}\lambda_0^3}\left[\frac{V_p}{V} n_p + \left(\frac{V - V_p}{V}\right) n_w\right]^3 \quad . \tag{3}$$

There, λ_0 is the vacuum wavelength of the lattice light, n_w the refractive index of water, and n_p that of the particles (here, $n_p = 1.59$). Since each elementary cell has four particles, for given particle radius, $R = 245$ nm, the particle-filled volume is known, $V_p = (16\pi/3)R^3$. Solving Eq. 3, we find a packing density $\frac{V_p}{V} = 43\%$. While this is lower than the maximum possible packing density (74%), it is larger than the maximum packing density of other structures (like the diamond structure, which has a maximum packing density of 34%). Therefore, the optical crystals prepared in this work are relatively dense. Further, the absolute number density of particles in the crystal, given by $4/V$, equals 7.1 μm^{-3}. In comparison, relatively dense, one-dimensional arrays have been formed previously in Ref. [13]. If their setup was generalized to 3D, the resultant density would be of order 0.3 μm^{-3}, *i.e.* about an order of magnitude lower than the density we estimate for our setup.

B. Trapping force

Another important quantity characterizing the usefulness of the optical crystal relies in the depth of the particle trapping potential and the trapping force. A simple estimate for the trapping potential, W, and the gradient force, $\mathbf{F} = -\nabla W$, for an isolated trapped particle can be made for particles with radius $R \ll \lambda$ [24], for which

$$W(\mathbf{r}) = -\frac{3V_1(n_\mathrm{p}^2 - n_\mathrm{w}^2)}{2c(n_\mathrm{p}^2 + 2n_\mathrm{w}^2)} I(\mathbf{r}) \quad , \tag{4}$$

where V_1 is the single-particle volume. In this approximation, the particles exhibit an isotropic, polarization-independent response to the field, and the back-action of the trapped particles onto the field is neglected. The trapping force in x-direction, which is measured in the experiment, follows from the maximum x-derivative of Eq. 2 and Eq. 4:

$$F_\mathrm{trap,x} = \frac{3V_1(n_\mathrm{p}^2 - n_\mathrm{w}^2)}{2c(n_\mathrm{p}^2 + 2n_\mathrm{w}^2)} \, 2\sqrt{2} I_0 K \quad . \tag{5}$$

Since in our case the particle radius is of order $\lambda/4$, the intensity gradient varies substantially over the particle volume, and Eq. 5 only yields an upper limit of the trapping force. An improved estimate is obtained by considering a trapping potential in which the intensity is averaged over the particle volume. This leads to an x-component of the gradient force:

$$F_\mathrm{x,av}(\mathbf{r}) = \frac{3(n_\mathrm{p}^2 - n_\mathrm{w}^2)}{2c(n_\mathrm{p}^2 + 2n_\mathrm{w}^2)} \int\limits_{\text{particle volume}} \left[\frac{\partial I(\mathbf{r}')}{\partial x'}\right] dx' \, dy' \, dz' \quad , \tag{6}$$

which depends on $\mathbf{r}$ via the particle volume. The corresponding trapping force is $F_\mathrm{trap,x,av} = \max_\mathbf{r} |F_\mathrm{x,av}(\mathbf{r})|$, evaluated along the path of easiest escape.

While the force measurement presented in Sec. IV is conducted with 2D crystals formed near the bottom cell wall, the laser configuration is identical with the configuration used to generate 3D crystals in the cell interior. Hence, we may assume that the optical trapping forces in the xy-plane are quite similar in the two cases. A comparison between the measured trapping force and the trapping forces that follow from Eqs. 5 and 6 is therefore in order.

For a single-beam power $P_0 = 350$ mW/4, an objective transmission $\eta = 0.6$ and an estimated beam cross section $A = (5\ \mu\mathrm{m})^2$, the single-beam intensity is $I_0 = \eta P_0/A = 2.1 \times 10^9$ W/m^2. For this intensity and the particle radius $R = 245$ nm used in the experiment, Eq. 5 yields a trapping force $F_\mathrm{trap,x} = 1.7$ pN, which exceeds the measured value of 0.42 pN by about a factor of four. Averaging the intensity gradient over the particle volume according to

Eq. 6 yields a trapping force $F_{\mathrm{trap,x,av}} = 0.45$ pN, which agrees very well with the experiment. Due to the uncertainty in the effective water viscosity used in the experimental analysis, the uncertainties in the intensity estimate, as well as the fact that the back action of the particles onto the field is neglected, the excellent level of agreement between $F_{\mathrm{trap,x,av}}$ and the measured force must be considered somewhat coincidental. Nevertheless, the comparison shows that our setup generates trapping forces of the expected order of magnitude. The same calculation also shows that the barrier height between adjacent lattice wells is $25k_{\mathrm{B}} \times$ 300 Kelvin. This result accords with the experimental observation that the optical lattice strongly suppresses the Brownian motion of particles trapped at a lattice site.

VI. CONCLUSION

Using a four-beam laser trap, we have obtained dense, light-induced, face-centered orthorhombic crystals of sub-micron particles in solution. The setup is very economical and may even be suitable for certain student labs. We have used a pair of Nikon E-Plan 100x, infinity-corrected objectives (cost about $400 each). There are no additional high costs, such as, for example, those associated with obtaining a spatial light modulator. The perfect mirror symmetry of the setup relative to the object plane considerably reduces the complexity of the optical alignment procedure: after aligning one of the four beams, the other three are fairly easy to align using the setup's symmetry. To our knowledge, the number density of the produced optical crystals is higher than previously achieved for a full 3D trap and for this particle size. Phase shifts of the laser beams have been used as a means of particle translation. The measured trapping force is within the expected range.

Since the interference patterns of multiple single-mode optical fields are inherently defect-free, the optical-lattice potentials derived from them are also defect-free. Further, for particles that are small enough to fit into the lattice wells, the single-site occupation probability approaches unity within the bulk of the optically induced crystals. Therefore, particle solutions containing only one type of suitable particles should result in optical crystals that are defect-free within the bulk of the crystal.

These properties point towards several future extensions and applications of the work. We intend to further study the static and dynamic crystallization behaviors for different lattice geometries and particle-to-wavelength aspect ratios. We already have observed that

lattice defects can be introduced artificially by simply adding a few impurity particles of significantly larger size; the role of impurities could be investigated further in the future. Exploring the effects of particle-particle and particle-field interactions in densely packed optical crystals will be another possibility. In the present work, we already have established that self-consistent modes of the combined particle-field system should exist, as we did not observe spontaneous disintegration of crystals. It is of theoretical interest to identify self-consistent solutions of the particle-field system, for large, densely packed particle ensembles. This could lead to applications of optical crystals as novel media with a tunable photonic bandgap.

Considering the high particle number densities of order $(\lambda/2)^{-3}$, it should be possible to use Bragg scattering of short-wavelength light or soft X-rays to measure particle localization and obtain structural information of non-spherical, strongly localized particles. Optical lattices with elliptical equipotential surfaces and/or additional static electric fields could be used to achieve alignment (in addition to localization). Extensions of the work along these lines may lead to studies of biological matter arranged in artificial crystals (bacteria, viruses, proteins).

We have deposited a movie that visualizes some of the contents of this paper [25].

ACKNOWLEDGMENTS

We acknowledge support by the NSF (PHY-0114336) and fruitful discussions with Professors P. Berman, C. Meiners and J. Ogilvie.

[1] P. S. Jessen and I. H. Deutsch, Adv. Atom. Mol. Opt. Phy. **37**, 95 (1996).

[2] N. V. Morrow and G. Raithel, Adv. Atom. Mol. Opt. Phy. **53**, 187 (2006).

[3] A. Ashkin, Phys. Rev. Lett. **24**, 156 (1970).

[4] A. Ashkin, Science **210**, 1081 (1980).

[5] A. Ashkin, J. M. Dziedzic, J. E. Bjorkholm, and S. Chu, Opt. Lett. **11**, 288 (1986).

[6] A. Jonáš and P. Zemánek, Electrophoresis **29**, 4813 (2008).

[7] M. Lang and S. Block, Am. J. Phys. **71**, 201 (2003).

[8] J.-M. Fournier, J. Rohner, P. Jacquot, R. Johann, S. Mias, and R.-P. Salath, Proc. SPIE - Int. Soc. Opt. Eng. **5930**, 59300Y (2005).

[9] M. M. Burns, J. M. Fournier, and J. A. Golovchenko, Science **249**, 749 (1990).

[10] A. E. Chiou, W. Wang, G. J. Sonek, J. Hong, and M. W. Berns, Opt. Comm. **133**, 7 (1997).

[11] M. P. MacDonald, L. Paterson, K. Volke-Sepulveda, J. Arlt, W. Sibbett, and K. Dholakia, Science **296**, 1101 (2002).

[12] A. N. Rubinov, V. M. Katarkevich, A. A. Afanas'ev, , and T. S. Efendiev, Opt. Comm. **224**, 97 (2003).

[13] A. Casaburi, G. Pesce, P. Zemanek, and A. Sasso, Opt. Comm. **251**, 393 (2005).

[14] M. Reicherter, T. Haist, E. U. Wagemann, and H. J. Tiziani, Opt. Lett. **24**, 608 (1999).

[15] D. G. Grier, Nature **424**, 21 (2003).

[16] J. Leach, G. Sinclair, P. Jordan, J. Courtial, M. Padgett, J. Cooper, and Z. Laczik, Opt. Exp. **12**, 220 (2004).

[17] H. Melville, G. Milne, G. Spalding, W. Sibbett, K. Dholakia, and D. McGloin, Opt. Exp. **11**, 3562 (2003).

[18] P. J. Rodrigo, V. R. Daria, and J. Gluckstad, Opt. Lett. **29**, 2270 (2004).

[19] H. J. Metcalf and P. V. der Straten, *Laser cooling and trapping* (Springer, New York, 1999).

[20] P. Zemánek, A. Jonáš, L. Šrámek, and M. Liška, Opt. Lett. **24**, 1448 (1999).

[21] J. A. Grieve, A. Ulcinas, S. Subramanian, G. M. Gibson, M. J. Padgett, D. M. Carberry, and M. J. Miles, Opt. Exp. **17**, 3595 (2009).

[22] W. H. Wright, G. J. Sonek, and W. M. Berns, Opt. Lett. **33**, 1735 (1994).

[23] L. P. Faucheux, G. Stolovitzky, and A. Libchaber, Phys. Rev. E **51**, 5239 (1995).

[24] K. C. Neuman and S. M. Block, Rev. Sci. Instr. **75**, 2787 (2004).

[25] See EPAPS Document No. [number will be inserted by publisher]